



[www.epj.org](http://www.epj.org)

Eur. Phys. J. E **26**, 369–377 (2008)

DOI: 10.1140/epje/i2007-10335-8

## Diffusing wave spectroscopy in Maxwellian fluids

J. Galvan-Miyoshi, J. Delgado and R. Castillo



Società  
Italiana  
Di Fisica



# Diffusing wave spectroscopy in Maxwellian fluids

J. Galvan-Miyoshi, J. Delgado, and R. Castillo<sup>a</sup>

Instituto de Fisica, Universidad Nacional Autonoma de Mexico, P. O. Box 20-364, Mexico, D. F. 01000, Mexico

Received 3 October 2007 and Received in final form 13 March 2008

Published online: 26 June 2008 – © EDP Sciences / Società Italiana di Fisica / Springer-Verlag 2008

**Abstract.** We present a critical assessment of the diffusing wave spectroscopy (DWS) technique for obtaining the characteristic lengths and for measuring the loss and storage moduli of a reasonable well-known wormlike micelle (WM) system. For this purpose, we tracked the Brownian motion of particles using DWS embedded in a Maxwellian fluid constituted by a wormlike micellar solution made of cetyltrimethylammonium bromide (CTAB), sodium salicylate (NaSal), and water. We found that the motion of particles was governed by the viscosity of the solvent at short times and by the stress relaxation mechanisms of the giant micelles at longer times. From the time evolution of the mean square displacement of particles, we could obtain for the WM solution the cage size where each particle is harmonically bound at short times, the long-time diffusion coefficient, and experimental values for the exponent that accounts for the broad spectrum of relaxation times at the plateau onset time found in the  $\langle \Delta r^2(t) \rangle$  vs. time curves. In addition, from the  $\langle \Delta r^2(t) \rangle$  vs. time curves, we obtained  $G'(\omega)$  and  $G''(\omega)$  for the WM solutions. All the DWS microrheological information allowed us to estimate the characteristic lengths of the WM network. We compare our DWS microrheological results and characteristic lengths with those obtained with mechanical rheometers at different NaSal/CTAB concentration ratios and temperatures.

**PACS.** 82.70.Uv Surfactants, micellar solutions, vesicles, lamellae, amphiphilic systems, (hydrophilic and hydrophobic interactions) – 82.70.Dd Colloids – 83.10.Pp Particle dynamics – 83.60.Bc Linear viscoelasticity

## 1 Introduction

Cationic surfactants in aqueous solutions in the presence of anionic benzyl hydrophobic moieties spontaneously self-assemble into long cylindrical, semiflexible micellar aggregates. Utilization of wormlike micelles (WMs) covers a wide spectrum of applications ranging from fracture fluids and drag reducing agents to templates for material systems [1]. The possibility of using “smart” WMs is exciting and promising [2]. The response of a fluid with wormlike aggregates to mechanical perturbation is viscoelastic [3, 4]. In the semidilute regime, where surfactant concentration is between the overlap concentration and a concentration where the mesh size,  $\xi$ , is larger than the persistence length,  $l_p$ , the linear rheology is dominated by reptation and by reversible breaking and recombination of the WMs. Two relaxation times related to these mechanisms  $\tau_{rep}$  and  $\tau_b$ , respectively, control the dynamic response. In these solutions, breaking time is shorter than reptation time [5]. Consequently, the relaxation modulus  $G(t)$  measured in stress relaxation experiments follows a Maxwellian behavior  $G(t) = G_0 \exp[-t/\tau_M]$ . Here,  $G_0$  is the plateau modulus related to the entanglement density of the micellar

mesh and  $\tau_M$  is a relaxation time equal to the geometric mean of  $\tau_{rep}$  and  $\tau_b$  [6]. This behavior is indeed so general that it is now admitted that a single relaxation time in the linear mechanical response is a strong indication of the wormlike character of self-assembled structures.

The response of any material to shear excitations is characterized by a complex shear modulus  $G^*(\omega)$  that determines the stress induced on a material upon application of an oscillatory shear strain at a frequency  $\omega$ . The real part of  $G^*(\omega)$ , the storage modulus  $G'(\omega)$ , is in phase with the applied shear strain. The imaginary part of  $G^*(\omega)$ , the viscous or loss component of the stress  $G''(\omega)$ , is in phase with the shear rate  $\dot{\gamma}$ . Regularly,  $G^*(\omega)$  is determined using mechanical rheometers, where viscoelastic properties are measured by application of strain while measuring stress or vice versa. However, in the last fifteen years, different techniques have been developed, usually named microrheology techniques [7], where micron-sized probe particles are embedded into the fluid to locally measure the viscoelastic response of the soft material. The response can be measured either by actively manipulating the probe particles or by passively measuring the mean square displacement ( $\langle \Delta r^2(t) \rangle$ ) of them, where the bulk mechanical susceptibility of the fluid determines the response of the probe particles excited by the thermal stochastic forces

<sup>a</sup> e-mail: rolandoc@fisica.unam.mx

which lead to Brownian motion.  $\langle \Delta r^2(t) \rangle$  can be related to  $G^*(\omega)$  by describing the motion of the particles with a generalized Langevin equation incorporating a memory function to take into account the viscoelasticity of the fluid. In this way, the particle fluctuation spectrum can be used to measure the relaxation spectrum of the fluid. Here, in contrast to mechanical rheometers, there is no strain applied on the material during the measurement. This is particularly useful in complex fluids where even small imposed strains can cause structural reorganization of the material and can change their viscoelastic properties. Various methods have been used to measure the displacement fluctuations of the embedded particles, such as video tracking [8–10] and diffusing wave spectroscopy (DWS) [11–13]. In the latter, dynamic light scattering (DLS) is used to measure the  $\langle \Delta r^2(t) \rangle$  of the probe particles.

In a DWS experiment, a laser beam strikes a slab formed by a turbid suspension made of the liquid under study and of the probe particles. The temporal autocorrelation function (ACF) of a small fraction of the light that passes through the slab is measured. The transport of light through the slab is treated as a diffusive process and photons are treated as random walkers, with a random walk step length equal to the transport mean free path  $l^*$  and a resultant diffusion coefficient  $D = vl^*/3$ , where  $v$  is the speed of light in the suspension. The diffusion approximation is valid for calculating transport of light only over distances longer than  $l^*$  [14]. When scattering is not isotropic, which is the case for particle sizes close to and larger than the photon wavelength, the random walk step length is longer than the photon mean free path length  $l$ . These lengths are connected by  $l^*/l = 2k_0^2/\langle q^2 \rangle$ , where  $k_0 = 2\pi n/\lambda$  is the photon wave vector in the solvent,  $\lambda$  is the laser wavelength in vacuum,  $n$  is the effective index of refraction in the sample, and  $\langle q^2 \rangle$  represents the angle average for the squared scattering vector for a typical scattering event experienced by the photon in the medium.  $l^*$  is a constant parameter that enters in the DWS analysis and has to be determined independently.

DWS microrheology was used for the first time in solutions of wormlike aggregates by van Zanten and Rufener [15]. They showed that experimentally observed  $\langle \Delta r^2(t) \rangle$  of polystyrene microspheres (diameter  $0.966 \mu\text{m}$ ) embedded in an aqueous solution of cetyltrimethylammonium bromide (CTAB) and KBr is well described, at long times by Brownian particles moving in a Maxwell fluid. Maxwell parameters were of the same order of magnitude as those obtained by mechanical rheology for similar systems; experimental details of the DWS technique were not given. Cardinaux *et al.* [16] studied concentrated aqueous solutions of hexa-ethylene glycol mono *n*-hexadecyl ether ( $\text{C}_{16}\text{E}_6$ ) that self-assemble in WMs at high surfactant concentration, using a combination of single- and multi-speckle DWS with polystyrene microspheres of two diameters ( $0.75 \mu\text{m}$  and  $1.5 \mu\text{m}$ ). Here, the authors have to use a factor of 1.52–2 of unknown origin to obtain a quantitative agreement between microrheology and classical rheometry. Bellour *et al.* [17] studied the aqueous solutions of hexane sulfonate cetyltrimethylammonium ( $\text{CTAC}_6\text{SO}_3$ ) and heptane sulfonate cetyltrimethylammo-

nium ( $\text{CTAC}_7\text{SO}_3$ ). These authors measured  $\langle \Delta r^2(t) \rangle$  for embedded polystyrene particles (diameter  $535 \text{ nm}$ ) in the semidilute regime and recognized three different regimes for the motion of the particles: a) At short times, the particles diffuse freely in the solvent with a Brownian dynamics, b) at intermediate times,  $\langle \Delta r^2(t) \rangle$  remains constant for a given time interval, and c) at longer times, the motion again becomes diffusive. Here, the long-time diffusion coefficient corresponds to the macroscopic viscosity of the solution. They were able to describe the entire  $\langle \Delta r^2(t) \rangle$  curve with an appropriate expression over 10 decades in time. They found a good agreement between the rheological parameters measured with DWS and those measured with mechanical rheology.

The purpose of this paper is to make a critical assessment of the DWS technique for obtaining the characteristic lengths and for measuring the loss and storage moduli of a reasonable well-known WM system. For this purpose, we tracked the Brownian motion of particles using DWS embedded in a Maxwellian fluid constituted by a wormlike micellar solution made of cetyltrimethylammonium bromide (CTAB), sodium salicylate (NaSal), and water. We found that the motion of particles was governed by the viscosity of the solvent at short times and by the stress relaxation mechanisms of the giant micelles at longer times. From the time evolution of the mean square displacement of particles, we could obtain for the WM solution the cage size where each particle is harmonically bound at short times, the long-time diffusion coefficient, and experimental values for the exponent that accounts for the broad spectrum of relaxation times at the plateau onset time found in the  $\langle \Delta r^2(t) \rangle$  vs. time curves. In addition, from the  $\langle \Delta r^2(t) \rangle$  vs. time curves, we obtained  $G'(\omega)$  and  $G''(\omega)$  for the WM solutions. All the DWS microrheological information allowed us to estimate the characteristic lengths of the WM network. We compare our DWS microrheological results and characteristic lengths with those obtained with mechanical rheometers at different NaSal/CTAB concentration ratios,  $R = [\text{NaSal}]/[\text{CTAB}]$ , and temperatures.

## 2 Diffusing wave spectroscopy

DWS is a multiple scattering technique, where  $\langle \Delta r^2(t) \rangle$  of probe particles is measured using time correlation functions. The time-averaged intensity ACF  $g_{(2)}(\tau)_t = \langle I(\tau)I(0) \rangle_t / \langle I(0) \rangle_t^2$ , where  $\langle \dots \rangle_t$  denotes time average, is obtained by collecting the scattered intensity from a single speckle over a sufficiently long collection period. The time-averaged field ACF,  $g_{(1)}(\tau)_t = \langle E(0)E^*(\tau) \rangle_t / \langle |E(0)|^2 \rangle_t$ , is related to the measured  $g_{(2)}(\tau)_t$  through the Siegert relation:  $g_{(2)}(\tau)_t = 1 + \beta |g_{(1)}(\tau)_t|^2$ , where  $\beta$  is an instrumental factor determined by collection optics. Time average is well defined if scattering properties of the medium are stationary. Within the diffusion approximation used in DWS for light transport in turbid media,  $\langle \Delta r^2(t) \rangle$  of a representative tracer particle is related to the ensemble averaged field ACF  $g_{(1)}(\tau)_e = \langle E(0)E^*(\tau) \rangle_e / \langle |E(0)|^2 \rangle_e$ , where  $\langle \dots \rangle_e$  is an average over the ensemble of speckles.

When all the scattering particles suspended in the medium are free to explore the same local environment during the course of a measurement, the scattering process is ergodic, and time-averaged and ensemble-averaged correlation functions are identical. In this case, all speckle fluctuation histories are equivalent and the traditional time-averaged DWS approach is valid.

## 2.1 Temporal intensity fluctuations of light

DWS theory connects temporal field fluctuations of the scattered light emerging from a turbid suspension to the dynamics of the particles embedded in the suspension. Here, photon path lengths are typically distributed over large distances and detected photons have been scattered many times at all possible angles. For the case in which all photons travel the same path length  $s$  along the sample  $g_{(1)}(\tau, s) = \exp[-\frac{2k_0^2 \langle \Delta r^2(\tau) \rangle (s/l^*)}{6}]$ . However, the measured ACF includes contributions from a distribution of path lengths,  $P(s)$ , and the result of the measurement is the weighted average [12]:

$$g_{(1)}(\tau) = \int_0^\infty P(s) \exp\left[-\frac{k_0^2 \langle \Delta r^2(\tau) \rangle}{3l^*} s\right] ds. \quad (1)$$

Equation (1) can be evaluated exactly [14] for the transmission of a plane wave through a slab of thickness  $L \gg l^*$  and infinite transverse extent, made of the scattering particles immersed in the liquid, using

$$g_1(\tau) = \frac{\frac{L/l^* + 4/3}{\alpha^* + 2/3} [\sinh[\alpha^* x] + \frac{2}{3} x \cosh[\alpha^* x]]}{(1 + \frac{4}{9} x^2) \sinh[\frac{L}{l^*} x] + \frac{4}{3} x \cosh[\frac{L}{l^*} x]}. \quad (2)$$

Here  $x = [k_0^2 \langle \Delta r^2(\tau) \rangle]^{1/2}$  and  $\alpha^* = z_0/l^*$ ;  $z_0$  is the distance into the sample from the incident surface to the place where the diffuse source is located. Therefore, measuring the intensity ACF  $g_2(\tau)$  allows us to obtain  $g_1(\tau)$  using the Siegert relation. If  $l^*$  and  $\alpha^*$  are known for the system,  $\langle \Delta r^2(t) \rangle$  can be obtained using equation (2).

*Estimation of  $\alpha^*$ .*  $\alpha^* = z_0/l^*$  can be estimated from a DWS experiment by fitting the intensity ACF for the back scattered light coming from a colloidal suspension made of particles of the same size as those to be used in the fluid to be investigated [18]. The intensity ACF can be given by

$$(g_2(t) - 1)_{pol} = \beta \exp\left[-2\gamma_{pol} \sqrt{\frac{6t}{\tau}}\right]. \quad (3)$$

Here, the subscript *pol* is used to indicate the polarization detection used in the experiment, *VV* for parallel and *VH* for cross polarization. Here,  $\tau = (k_0^2 D)^{-1}$  is the relaxation time and  $D$  is the diffusion coefficient, and  $\gamma_{pol} = \alpha_{pol}^* + 2/3$ . As  $D$  is known,  $\alpha^* \equiv \langle \alpha^* \rangle = (\alpha_{VV}^* + \alpha_{VH}^*)/2$  can be determined by fitting the intensity ACF.

## 2.2 Brownian motion and microrheology in a Maxwell fluid

The standard Langevin description for a particle of mass  $m$  immersed in a complex fluid undergoing Brownian motion has been modified to include viscoelastic effects [19], using a time-dependent memory function:

$$m \frac{d\mathbf{v}}{dt}(t) = - \int_0^t \zeta(t-t') \mathbf{v}(t') dt' + \mathbf{f}_R(t). \quad (4)$$

Here,  $\mathbf{v}(t)$  is the particle velocity and  $\mathbf{f}_R(t)$  denotes the random Brownian or thermal forces acting on the particle.  $\zeta(t)$  is the Maxwellian fluid time-dependent memory function that accounts for both energy loss and storage upon deformation. The ability to store energy upon deformation changes the temporal correlations of the stochastic forces acting upon the particle at thermal equilibrium, since the suspending medium must satisfy the fluctuation dissipation theorem  $\langle \mathbf{f}_R(t) \cdot \mathbf{f}_R(0) \rangle = k_B T \zeta(t)$ ;  $k_B$  is the Boltzmann constant. If we assume  $\tilde{\eta}(s) = \tilde{\zeta}(s)/6\pi a$ , where  $s$  is the frequency in the Laplace domain and  $a$  is the particle radius, the relation between  $\tilde{G}(s)$  and  $\langle \Delta \tilde{r}^2(s) \rangle$  can be written as [19]

$$\tilde{G}(s) = \frac{s}{6\pi a} \left[ \frac{6k_B T}{s^2 \langle \Delta \tilde{r}^2(s) \rangle} - ms \right]. \quad (5)$$

Using the unilateral Fourier transform,  $\mathfrak{F}_u\{\langle \Delta r^2(t) \rangle\}(\omega)$ , and neglecting the second term of equation (5), an expression for the viscoelastic modulus as a function of frequency can be obtained:

$$G^*(\omega) = \frac{1}{\pi a} \frac{k_B T}{i\omega \mathfrak{F}_u\{\langle \Delta r^2(t) \rangle\}(\omega)}. \quad (6)$$

Several procedures have been followed by different authors [15, 19, 20] to determine  $\mathfrak{F}_u\{\langle \Delta r^2(t) \rangle\}(\omega)$ . In our case, numerical inversion of equation (2) allowed us to obtain  $\langle \Delta r^2(t) \rangle$ , where  $g_1(\tau)$  is calculated from the experimental curve  $g_{(2)}(\tau)$  using the Siegert relation. Instead of making any transformation of  $\langle \Delta r^2(t) \rangle$  vs.  $t$  curve, we first fitted the curve to a model curve proposed by Bellour *et al.* [17], for describing  $\langle \Delta r^2(t) \rangle$  over 8-10 decades in time for colloidal particles in Brownian motion embedded in a WM solution. The model curve is given by

$$\langle \Delta r^2(t) \rangle = 6\delta^2 \left(1 - e^{-\left(\frac{D_0}{\delta^2} t\right)^\alpha}\right)^{1/\alpha} \left(1 + \frac{D_m}{\delta^2} t\right). \quad (7)$$

Here,  $6\delta^2$  is the value of  $\langle \Delta r^2(t) \rangle$  at the plateau,  $D_0$  is the diffusion coefficient for particles in the solvent at infinite dilution and  $D_m$  is the diffusion coefficient for the particles for long times. To obtain the real and complex components of  $G^*(\omega)$ , we calculated the Laplace transform of the computed fitting curve and after transforming  $s \rightarrow i\omega$  (analytic continuity), we introduced it in equation (6).

## 3 Experimental section

*Materials.* Cetyltrimethylammonium bromide (CTAB; > 99%) was purchased from Fluka Chemie gmbH (Germany) and sodium salicylate (NaSal; 99.5%) from Sigma-Aldrich (MO, USA). All of them were used without further

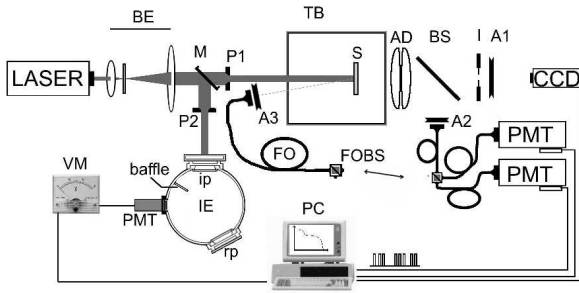


**Fig. 1.** Schematic diagram of the DWS instrument. A laser beam is sent through a filter and a beam expander (BE). Afterwards the beam is deviated depending on the kind of experiment to be done by a mirror (M). In the case of  $l^*$  measurements, the beam is sent into the sample and the scattered light is collected by the integrating sphere. In the case of DWS measurements, the beam is sent into the sample (S) that is in a temperature-controlled bath (TB). The scattered light is collected, with the aid of an achromatic doublet (AD) and a beam splitter (BS), by a couple of photomultipliers in cross correlation and by a CCD camera to make multispeckle DWS.

purification. Polystyrene microspheres of different diameters were used as tracers in DWS experiments (Bangs Labs Inc, USA). Glass cells were supplied by Hellma GmbH (Germany) and by Starna cells Inc (USA) with different optical paths (2 mm to 4 mm) and different cross sections ( $3.0 \times 4.2$  mm and  $2.8 \times 3.7$  mm). Water was milli-Q water (Nanopure-UV, USA; 18.3 M $\Omega$ ).

*Instrument.* Our DWS setup is a home-made instrument shown schematically in Figure 1. A laser beam (Coherent Innova 300, Coherent Inc, USA) is filtered and subsequently expanded to avoid sample heating and to assure plane wave approximation. The beam is sent at normal incidence on a square cell where the WM solution samples with the 800 nm diameter microspheres that multiply scatter light are placed. The scattered light is collected by photomultiplier tubes (Thorn EMI, England) through polarizing maintaining optical fibers from OZoptics Inc (USA). Signals are converted into TTL pulses using ALV preamplifiers (ALV GmbH, Germany) and processed by an ALV/5000E multi-tau correlator (ALV GmbH, Germany) to obtain the intensity ACFs; most of our work was done in transmission geometry. An integrating sphere (Oriental Newport, USA) is also included in our instrument to obtain  $l^*$  for colloidal suspensions. In addition, we included a CCD camera to make multispeckle DWS in transmission geometry. Multiply scattered light is collected by a pair of achromatic doublets (Edmund Optics Inc., NJ, USA), which image the transmitted light 1 to 1 on a plane where a diaphragm is placed to control the speckle size [21]. A TM-6710CL Pulnix CCD camera (JAI Inc., USA) is located at ca. 20 cm from the diaphragm. Images are acquired at 120 fps by a BitFlow R64 frame Grabber (BitFlow Inc., MA USA) and real time processed with a Pentium IV PC running at 2.8 MHz. The time ACFs were calculated using the algorithm proposed by Viasnoff *et al.* [21]. Time over-

lap between DWS and multispeckle DWS is around 4 orders of magnitude and measurement times about 18000 s.

*Sample preparation.* The CTAB/NaSal/water micellar solution is in a good approximation a Maxwell fluid at low and intermediate frequencies [3]. All micellar solution samples were prepared by weight, where the CTAB concentration was maintained constant at  $\sim 0.1$  M and the NaSal concentration was varied from  $\sim 0.04$  M to 0.4 M to sweep several  $R$  values. Because micellar solution viscosity is high at room temperature and to avoid colloidal agglomeration, we followed a two-step procedure. In the first step, water, CTAB and NaSal were mixed. Solutions were left for 48 hours to relax. In the second step, the samples placed in sealed cells to avoid water evaporation were heated to 50 °C to reduce viscosity. Then, microspheres in water suspension (10%) were added while stirring the samples. Stirring was maintained for 20 minutes and subsequently samples were sonicated for another 15 minutes to assure a homogeneous dispersion. Samples were allowed to relax for 14 days at 30 °C. To avoid interparticle interactions, as well as hydrodynamic correlation, particle volume fractions ranged between 0.013 and 0.016.

*Transport mean free path.* We used a precise method to obtain  $l^*$  from transmittance and reflectance measurements of the samples to be investigated, using an integrating sphere. This method is described elsewhere [22]. Just to assess the quality of our  $l^*$  measurements for colloidal suspensions of particles with different sizes, we calculated  $l^*$  using Mie scattering theory following the procedures developed by several authors [23–25]. The agreement between  $l^*$  measured using the method employing the integrating sphere and  $l^*$  calculated with Mie scattering theory is excellent. There is just a 3.8% mean deviation between theory and experiment. Also, we measured  $l^*$  using DWS in transmission geometry for suspensions where the properties of the particles are known. Here,  $g_1(\tau)$  was obtained for water suspensions made of particles with a known diameter and refractive index (1.59 at 514.5 nm). In this case, microspheres moving in Brownian motion follow the Einstein equation for hard-spheres corrected for concentration [26], *i.e.*  $D = (k_B T / 6\pi\eta_w a)(1 - 1.83\phi + 0.88\phi^2) = \langle \Delta r^2(\tau) \rangle / 6t$ , where  $\eta_w$  is the water viscosity. Therefore, using this  $\langle \Delta r^2(\tau) \rangle$  and the known values for  $a$  and  $L$  allowed us to calculate  $l^*$  as a free parameter fitting the experimental  $g_1(\tau)$ . The mean deviation between the measured  $l^*$  using the integrating sphere and DWS was less than 2.5%.

*Rheometric measurements.* They were carried out in a cone-plate cell (4°, diameter 40 mm) with controlled temperature using a Bohlin Gemini HRnano rheometer (Malvern, UK). Oscillatory strain amplitude was 0.1.

## 4 Results and discussion

In this section, we present the results for the  $\langle \Delta r^2(t) \rangle$  as a function of time for microspheres embedded in the WM solutions using DWS. From these curves, we obtained several parameters useful to understand the worm-micelle

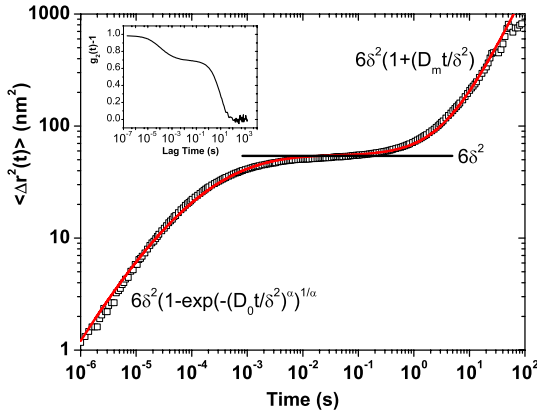


**Fig. 2.** Typical curve for the  $\langle \Delta r^2(t) \rangle$  as a function of time. Open squares correspond to  $\langle \Delta r^2(t) \rangle$  obtained from numerical inversion of the light intensity ACF (shown in the inset) obtained by DWS. The continuous line corresponds to the best-fit curve using the model given by Bellour *et al.* [17]. The mathematical expressions correspond to the factors in the model that dominates at those time scales.

network in the CTAB/NASal/water system, which can be compared with those obtained with other techniques. In addition, the elastic and loss moduli for the WM solutions as a function of frequency were calculated from the  $\langle \Delta r^2(t) \rangle$  for different NaSal/CTAB ratios and temperatures. These moduli are compared with those obtained with mechanical rheometric measurements. The DWS microrheological data allowed us to estimate the characteristic lengths of the MWs and to compare them with those obtained with other techniques.

#### 4.1 Mean square displacement in a solution of wormlike micelles

Figure 2 shows a typical mean square displacement curve *vs.* time (more than eight orders of magnitude) for 800 nm diameter microspheres dispersed into a micellar solution of the system CTAB/NaSal/water. The experimental points are the result of numerical inversion of equation (2), where  $g_1(\tau)$  came from a DWS experiment. The light intensity ACF that originated these  $\langle \Delta r^2(t) \rangle$  is shown in the inset. Multispeckle DWS in transmission geometry was used to assure that sampling was ergodic. To get the rheological parameters for the WM solutions to be shown below, instead of making the Laplace transform on the experimental points coming from the numerical inversions, first, we fitted them with the model proposed by Bellour *et al.* [17] for describing the mean square displacement of colloidal particles in a WM fluid (Eq. (7)); afterwards, the Laplace transformation was done on those best-fit functions. In our procedure, we left as free parameters  $\delta$ ,  $D_m$  and  $\alpha$ ; since  $D_0$  corresponds to diffusion in pure water. The best-fit function for the  $\langle \Delta r^2(t) \rangle$  data is also shown in Figure 2 as a continuous line; we can observe that the fitting is excellent. We observe in this figure three different regimes for the motion of particles, which are shared by all mi-

**Table 1.** Fitting parameters for the  $\langle \Delta r^2(t) \rangle$  for different values of  $R$  and temperature.

$R$	$6\delta^2$ (nm <sup>2</sup> )	$D_m$ (nm <sup>2</sup> /s)	$\alpha$	$T$ (°C)
0.4	71.1	0.19	0.26	20
0.4	84.4	0.51	0.26	22
1.0	51.2	8.72	0.24	22
1.0	49.9	20.11	0.26	25
1.5	54.6	2.51	0.25	20
1.5	56.0	3.68	0.25	22
1.5	47.7	10.84	0.25	25
2.0	34.1	0.58	0.23	20
2.0	35.4	0.81	0.23	22
2.0	41.7	2.33	0.24	25
4.0	46.8	8.07	0.24	22

cellar solutions [15–17]. At short times, there is a regime where  $\langle \Delta r^2(t) \rangle$  is almost a linear function of time, at intermediate times  $\langle \Delta r^2(t) \rangle$  remains constant for a given time interval (a plateau), and at longer times  $\langle \Delta r^2(t) \rangle$  is again a linear function of time. These regimes are present in our micellar system no matter the NaSal/CTAB ratio or the temperature.

The model given by equation (7) was originally thought for Brownian particles harmonically bound around a stationary mean position, as a consequence  $\langle \Delta r^2(t) \rangle = 6\delta^2(1 - e^{-(\frac{D_0}{\delta^2}t)})$ , where the particle's amplitude of the motion, *i.e.* the cage size  $\delta$ , is related to the plateau modulus  $G_0 = k_B T / (6\pi a \delta^2)$ ; this can be easily obtained substituting  $\langle \Delta r^2(t) \rangle$  in equation (5). However, this cage where particles are momentarily trapped fluctuates due to the breaking/reptation process. Thus, the particles are bound to their mean position on time scales smaller than the longest characteristic time of the micellar system,  $\tau_M = \eta_m / G_0$  [6], where  $\eta_m$  is the long-time viscosity of the system. Therefore, to get  $\langle \Delta r^2(t) \rangle = 6D_m t$  at long times, it was proposed that  $\langle \Delta r^2(t) \rangle = 6\delta^2(1 - e^{-(\frac{D_0}{\delta^2}t)})(1 + \frac{D_m}{\delta^2}t)$ . However, this expression did not describe correctly the dynamics at the plateau onset time, because dynamics of the particles exhibits a very broad time relaxation spectrum [17]. This led to include the parameter  $\alpha$  as shown in equation (7), where  $\alpha = 1$  indicates monoexponential relaxation; the smaller  $\alpha$  the larger relaxation spectrum.

Table 1 summarizes the fitting parameters for the  $\langle \Delta r^2(t) \rangle$  of microspheres dispersed in the different micellar solutions where  $R$  and temperature were varied. The first thing to be noticed is that the  $\alpha$  values for our system are very close to those found for the WM solutions of CTAC<sub>7</sub>SO<sub>3</sub> [17]. Therefore, in both systems, the dynamics of the particles at the plateau onset time shows a similar broad relaxation spectrum.  $\delta^2$  values for all the micellar solutions are on the average close to 8.7 nm<sup>2</sup>. In Table 1, we present  $6\delta^2$  values that are more useful for interpretation. The  $6\delta^2$  values for micellar solutions at  $R = 0.4$  are to some extent larger than the  $6\delta^2$  average,  $\langle 6\delta^2 \rangle$ , for all the micellar solutions studied here

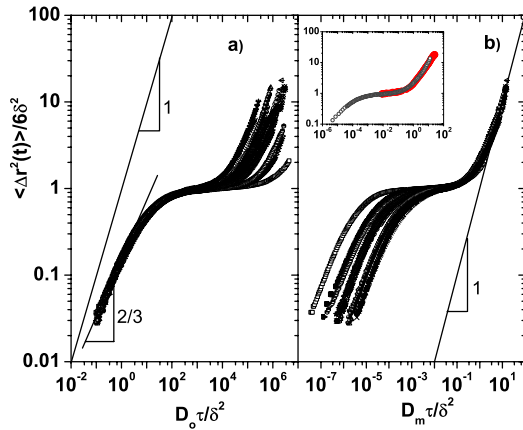


**Fig. 3.** (Colour on-line) Universal curves for different time scales. a)  $\langle \Delta r^2(t) \rangle / 6\delta^2$  vs.  $D_0 t / \delta^2$ , subdiffusive regime with a slope of 2/3. b)  $\langle \Delta r^2(t) \rangle / 6\delta^2$  vs.  $D_m t / \delta^2$ , diffusive regime with a slope of 1. Inset shows the overlap between DWS (Hollow, grey symbols) and Multispeckle DWS (solid, red symbols) experimental points.

( $6\delta^2$ )  $\sim 52.1 \text{ nm}^2$ ). On the contrary for  $R = 2$ , the  $6\delta^2$  values are slightly below that average. To compare our cage size results with those obtained for the case of WMs in the CTAC<sub>7</sub>SO<sub>3</sub>/water system at different surfactant concentrations, we fitted and interpolated the  $6\delta^2$  values given in reference [17]. For a surfactant concentration similar to that used in our solutions ( $\sim 3.6\%$ ),  $6\delta^2 \sim 51 \text{ nm}^2$  was obtained for CTAC<sub>7</sub>SO<sub>3</sub>. This value agrees well with our  $\langle 6\delta^2 \rangle$ . The diffusion coefficient for long times,  $D_m = k_B T / 6\pi a \eta_m$ , is dominated by the long-time viscosity. As is well known, viscosity as a function of  $R$  presents two maximums ( $\sim R = 0.6$  and  $R = 1.24$ ) and one minimum ( $\sim R = 1.02$ ) [27–29]; the behavior of  $D_m$  follows this trend but in an inverse form. As temperature increases  $D_m$  also increases because  $\eta_m$  decreases with temperature following an Arrhenius behavior [30].

In Figure 3a, we present the  $\langle \Delta r^2(t) \rangle$  rescaled by the cage size of the colloidal particles,  $6\delta^2$ , vs. time, which is rescaled by the longest relaxation time of the Rouse modes in the Zimm model  $\tau_R = \delta^2 / D_0$ , i.e.,  $\langle \Delta r^2(t) \rangle / 6\delta^2$  vs.  $D_0 t / \delta^2$ . Here, we show that no matter the NaSal/CTAB ratio or the temperature, we get a universal behavior for  $t \ll \tau_R$  where particles are moving in a sub-diffusive motion, which follow  $\langle \Delta r^2(t) \rangle \sim t^{2/3}$  for more than a decade in good agreement with the Zimm model [31, 32]. In Figure 3b, an equivalent scaling could give also a universal behavior for long times. Here,  $\langle \Delta r^2(t) \rangle$  is rescaled by  $6\delta^2$  and time by the longest characteristic time of the micellar system  $\tau_M = \delta^2 / D_m$ . In the same way as before, no matter the values of  $R$  or of  $T$  a universal curve is obtained; however here, the slope of this universal curve is one, according to equation (7) for long times.

In Figures 4a and b, we present the elastic (real part) and the viscous (imaginary part) components of the complex modulus  $G^*$ . Figure 4a shows  $G'$  and  $G''$  for  $R = 1.5$  at different temperatures: 20 °C, 22 °C and 25 °C, and Figure 4b shows the same variables when the ratio is var-

ied, i.e.,  $R = 0.4, 1.0$  and  $2.0$  and temperature is constant 22 °C. As we can observe from Figures 4a and b, the agreement between those moduli obtained using DWS and those using mechanical rheometry is quite well, at low and intermediate frequencies. When using micron-sized probes, probe and solvent inertial effects are negligible up to frequencies of  $\omega \sim 10^5 \text{ rad/s}^{-1}$ . Therefore, DWS microrheology achieves a bandwidth far beyond that of conventional rheometers allowing to observe two crossovers, as can be observed in Figures 4a and b. As is well known, our fluid is constituted by WMs. Here, stress relaxation occurs via reptation and scission. In the fast breaking limit, this stress relaxation leads to a single relaxation time and to a Maxwellian behavior at low and intermediate frequencies. The plateau modulus and the relaxation time can be obtained from the first crossover. On time scales shorter than the breakage time of micelles, the Maxwellian stress relaxation process is essentially frozen and the micelles can be regarded as semiflexible chains. Therefore, in the high-frequency regime stress relaxes via intramicellar processes: First dominated by the Rouse-Zimm modes and then by the internal relaxation of individual Kuhn segments. In this frequency range,  $G^*$  exhibits a power law behavior,  $G^* \sim \omega^\nu$ , with the exponent  $\nu$  changing from approximately 5/9 in the Rouse-Zimm regime to 3/4, where internal bending modes of Kuhn segments dominate. The change occurs around a critical frequency  $\omega_0$  corresponding to the shortest relaxation time in the Rouse-Zimm spectrum. One important feature to be pointed out is about the local minimum of  $G''(\omega)$ . This is usually better defined in DWS microrheology than in mechanical rheometry. As a consequence in Cole-Cole plots,  $G''$  vs.  $G'$ , the corresponding frequency for this minimum is more accurately determined with DWS microrheology (see inset in Fig. 4a). This is important for estimating the characteristic lengths of the WM solution, as shown below.

The comparison of mechanical rheological data from different authors in WM systems is not an easy task. In these systems measurement protocols play a central role. In particular, it is well known that cell geometry, cell parameters, sample preparation, and even different reactive stocks have been described as factors that could introduce large deviations in WM rheology. In particular, it is important to note that mechanical rheology measurements of  $G_0$  for different nominally identical samples have an error bar  $\sim 20\%$ ; for relaxation times the error bar is  $\sim 5\%$ . As we will see, DWS microrheology seems to share some kind of these problems (WM sample preparation, probe particle dispersion). So, this has to be considered when DWS microrheology and mechanical rheology are compared. In Table 2, we present a typical example of the plateau modulus and the relaxation time obtained from the first crossover (intermediate frequencies) in the  $G'$  and  $G''$  vs.  $\omega$  plots determined using DWS microrheology and those obtained with a mechanical rheometer. Although the agreement between them is good, it is not excellent. For the Maxwell relaxation times, microrheology and mechanical rheology give numbers of the same order of magnitude, with a similar dispersion to the relaxation times obtained between different authors using just mechanical rheology. In all the

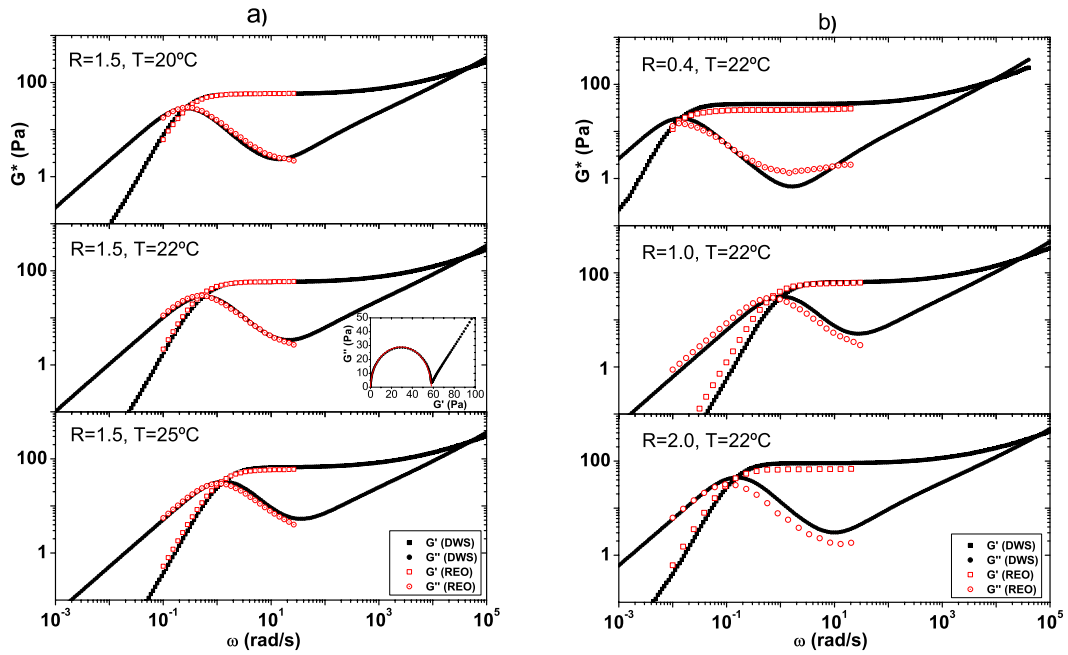


**Fig. 4.** The elastic,  $G'$ , and the viscous,  $G''$ , components of the complex modulus for the CTAB/NaSal/water system at different temperatures and fixed  $W = 1.5$  (a). Inset: Cole-Cole plot from DWS microrheology (line: best fit for Maxwell model). b) At different  $W$  values and fixed  $T = 22^\circ\text{C}$ .

**Table 2.** Plateau modulus and Maxwell relaxation time at  $T = 22^\circ\text{C}$ .

$R$	Plateau modulus, $G_0$ (Pa)		Maxwell relaxation time, $\tau_M$ (s)	
	Microrheology	Rheometry	Microrheology	Rheometry
0.4	38.7	28.9	70.2	82.6
1.0	63.5	60.2	0.9	1.4
1.5	58.3	58.5	1.8	2.0
2.0	90.5	67.2	6.5	9.2
4.0	68.0	45.7	1.0	0.5

cases, the higher temperature, the lower relaxation time for all  $R$  values. This is a reliable feature observed in relaxation times when mechanical rheology is used varying temperature. DWS microrheology usually overestimates  $G_0$ , although it follows the same trend as  $R$  is varied. The best agreement between rheology and microrheology occurs around  $R \sim 1$ – $1.5$ . At larger  $R$  values, the difference gets worse. One possible reason for this behavior is that the large quantity of free ions ( $\text{Sal}^-$ ) in the solution, not incorporated into the micelles, could modify the mobility of the Brownian particles or even the topology of the WMs [33].

With the obtained DWS microrheological results, it is possible to estimate the most important characteristic lengths in the CTAB/NaSal WM solution. It is important to mention that theory developed for WMs is far from being complete, however it could be interesting to evaluate using approximate relations, the characteristic lengths in the system under study here as  $R$  and temperature are varied. We present these estimated characteristic lengths in Table 3. The mesh size,  $\xi = (k_B T / G_0)^{1/3}$  [31, 34], for our micellar solutions is in the range of 35–45 nm. Using

our mechanical rheological data,  $\xi$  ranges from 39–53 nm. The microrheological derived mesh size agrees well with reported values in the literature, where we can find values of  $\xi = 40$  nm for  $R = 2$  [35], and  $\xi = 45$  nm for  $R = 2$  and  $R = 1.5$ , at  $25^\circ\text{C}$  [36]. As we can observe,  $\xi$  is little bit lower than the reported values, since  $G_0$  is overestimated in DWS microrheology. The persistence length of the WMs can be deduced directly from  $\omega_0 \approx k_B T / 8\eta_m l_p^3$  [37], which is the frequency, where the exponent  $\nu$ , in  $G^*(\omega) \sim \omega^\nu$ , changes from  $5/9$  to  $3/4$  as mentioned above. Our values for  $l_p$ , ranging from 29 to 45 nm, are of the same order of those found by other authors for the same system. For example,  $l_p = 23.5$  nm as given by Nettesheim and Wagner [35] and  $l_p = 36$ – $38$  nm in the dilute regime as given by Berret [3]. In general,  $l_p$  is not sensible to  $R$  [3] and CTAB concentration [35]. The contour length of the WMs,  $L_C$ , can be obtained from the equation  $G''_{\min}/G_0 \approx l_e/L_C$  as given by Granek and Cates [38]. It is important to note that  $G''_{\min}/G_0$  is much less than 0.1 for most of our cases [38], therefore this ratio produces relatively good values for  $l_e/L_C$ . Here,  $l_e$  is

**Table 3.** Characteristic lengths for the CTAB/NaSal/water system at different  $R$  values and temperatures obtained using DWS microrheology.

$R$	$T$ (°C)	$\xi$ (nm)	$G''_{\min}$ (Pa)	$\omega_0$ (s <sup>-1</sup> )	$l_p$ (nm)	$l_e$ (nm)	$L_C$ (nm)
0.4	20	45	0.48	10176.7	36	51	4865
0.4	22	47	0.66	5383.8	45	49	2782
1.0	22	40	5.09	129583.3	34	75	933
1.0	25	40	6.97	19078.5	30	48	455
1.5	20	41	2.36	19618.8	29	51	1282
1.5	22	41	3.39	19555.6	29	52	884
1.5	25	39	5.33	19912.6	29	47	612
2.0	20	35	2.46	19865.3	29	39	1517
2.0	22	35	3.04	19805.1	29	40	1216
2.0	25	37	3.96	19521.0	29	44	869
4.0	22	39	5.57	13931.8	33	46	408

the contour length between two entanglements, which is computed using  $l_e \approx \xi^{5/3}/l_p^{2/3}$  [38] and  $G''_{\min}$  is the minimum in the  $G''$  vs.  $\omega$  plot.  $l_e$  from our DWS data ranges between 39–75 nm. In particular, for the case of  $R = 2$ , our  $l_e$  values ranges from 39–44 nm, which is smaller than  $l_e = 55$  nm reported in reference [35] using mechanical rheology. The underestimation for  $\xi$  is probably the reason behind our low DWS  $l_e$  values.  $L_C$  ranges from approximately 400 nm to 4800 nm depending on  $R$  and  $T$  values. The larger the temperature, the smaller  $L_C$ . This length gives us an order of magnitude of the size of the WMs in this system. In particular, for  $R = 2$  using dynamical rheology,  $L_c = 1600$  nm [35], in contrast, using DWS our values range from 869–1517 nm depending on temperature.

We consider that the underlying reason of the good agreement between mechanical rheometry and DWS microrheology is because the relevant micellar solution scale lengths in the micellar solution, as the mesh size, entanglement length, etc. are not larger than the probe particle radius. Thermal motion of a single particle reflects the viscoelastic properties of its environment on roughly the scale of the probe particle radius, since this is the length scale on which the strain-field around the particle decays, and how such a perturbation propagates into the system depends on the characteristic lengths of the material in relation to the probe size. DWS experiments with different probe diameters (0.5–3  $\mu\text{m}$ ) have been reported in the literature [17].

## 5 Conclusion

We employed diffusing wave spectroscopy to probe the motion of particles embedded in semi-dilute solutions of WMs in the system cetyltrimethylammonium bromide, sodium salicylate, and water. We showed that the motion of particles is governed at very short times by the viscosity of the solvent and by stress relaxation mechanisms in the micellar network at longer times. We obtained from the mean square displacement of particles vs. time curves, the viscoelastic properties of the system at

different CTAB/NaSal ratios and temperatures. We made a critical evaluation of the DWS technique for obtaining the characteristic lengths and for measuring the loss and storage moduli in a reasonable well-known WM system. In general, DWS microrheology results agree relatively well with mechanical rheometry results and they show the same kind of data dispersion. Although, DWS allows to reach high-frequency values for the rheological moduli, which is not possible to do with standard rheometers.

The support from SEP-CONACYT (46778) and DGAPA UNAM (IN110505) is gratefully acknowledged. J.D. and J.G.-M. thank CONACYT (166853, 159882) and DGEP UNAM for financial support. We thank to C. Garza and S. Ramos for their technical support.

## References

1. W.J. Kim, S. Yang, Chem. Mater. **12**, 3227 (2000).
2. S. Esrahi, E. Tuval, A. Aserin, Adv. Colloid Interface Sci. **77**, 128 (2006).
3. J.F. Berret, *Rheology of wormlike micelles: Equilibrium Properties and Shear Banding Transitions*, in *Molecular Gels. Materials with Self-Assembled Fibrillar Networks*, edited by R.G. Weiss, P. Terech (Springer, The Netherlands, 2006) p. 663.
4. L.M. Walker, Curr. Opin. Colloid Interface Sci. **6**, 451 (2001).
5. M.E. Cates, S.J. Candau, J. Phys.: Condens. Matter **2**, 6869 (1990).
6. M.E. Cates, Macromolecules **20**, 2289 (1987).
7. F.C. MacKintosh, C.F. Schmidt, Curr. Opin. Colloid Interface Sci. **4**, 300 (1999).
8. T. Gisler, D.A. Weitz, Curr. Opin. Colloid Interface Sci. **3**, 586 (1998).
9. A. Mukhopadhyay, S. Granick, Curr. Opin. Colloid Interface Sci. **6**, 423 (2001).
10. D.T. Chen, E.R. Weeks, J.C. Crocker, M.F. Islam, R. Verna, J. Gruber, A.J. Levine, T.C. Lubensky, A.G. Yodh, Phys. Rev. Lett. **90**, 108301 (2003).
11. G. Maret, P.E. Wolf, Z. Phys. B **65**, 409 (1987).

12. D.J. Pine, D.A. Weitz, P.M. Chaikin, E. Herbolzheimer, *Phys. Rev. Lett.* **60**, 1134 (1988).
13. J.L. Harden, V. Viasnoff, *Curr. Opin. Colloid Interface Sci.* **6**, 438 (2001).
14. D.A. Weitz, D.J. Pine, in *Dynamic Light Scattering*, edited by W. Brown (Oxford University Press, New York, 1993), Chapt. 16, pp. 652–720.
15. J.H. van Zanten, K.P. Rufenner, *Phys. Rev. E* **62**, 5389 (2000).
16. F. Cardinaux, L. Cipelletti, F. Scheffold, P. Schurtenberger, *Europhys. Lett.* **57**, 738 (2002).
17. M. Bellour, M. Skouri, J.-P. Munch, P. Hebraud, *Eur. Phys. J. E* **8**, 431 (2002).
18. F. Scheffold, *J. Dispersion, Sci. Technol.* **23**, 591 (2002).
19. T.G. Mason, D.A. Weitz, *Phys. Rev. Lett.* **74**, 1250 (1995).
20. B.R. Dasgupta, S.Y. Tee, J.C. Crocker, B.J. Frisken, D.A. Weitz, *Phys. Rev. E* **65**, 51505 (2002).
21. V. Viasnoff, F. Lequeux, D.J. Pine, *Rev. Sci. Instrum.* **73**, 2336 (2002).
22. J. Galvan-Miyoshi, R. Castillo, to be published in *Rev. Mex. Fis.* (2008).
23. L.F. Rojas-Ochoa, D. Lacoste, R. Lenke, P. Schurtenberger, F. Scheffold, *J. Opt. Soc. Am. A* **21**, 1799 (2004).
24. A. Ishimaru, *Wave Propagation and Scattering in Random Media* (Academic Press, New York, 1978).
25. H.C. van de Hulst, *Light Scattering by Small Particles* (Dover, New York, 1981).
26. G.K. Batchelor, *J. Fluid Mech.* **74**, 1 (1976).
27. H. Azzouzi, J.P. Decruppe, S. Lerouge, O. Greffier, *Eur. Phys. J. E* **17**, 507 (2005).
28. H. Rehage, H.J. Hoffmann, *Phys. Chem.* **92**, 4712 (1988).
29. R. Gamez-Corrales, personal communication.
30. F. Kern, R. Zana, S.J. Candau, *Langmuir* **7**, 1344 (1991).
31. P.G. de Gennes, *Scaling Concepts in Polymer Physics* (Cornell University Press, Ithaca, 1979).
32. W. Jiang, J. Huang, Y. Wang, M. Laradji, *J. Chem. Phys.* **126**, 44901 (2007).
33. W.J. Briels, P. Mulder, W.K. den Otter, *J. Phys: Condens. Matter* **16**, S3965 (2004).
34. M. Doi, S.F. Edwards, *The Theory of Polymer Dynamics* (Clarendon, Oxford, 1986).
35. F. Nettesheim, N.J. Wagner, *Langmuir* **23**, 5267 (2007).
36. T. Shikata, S.J. Dahman, D.S. Pearson, *Langmuir* **10**, 3470 (1994).
37. N. Willenbacher, C. Oelschlaeger, M. Schopferer, P. Fischer, F. Cardinaux, F. Scheffold, *Phys. Rev. Lett.* **99**, 68302 (2007).
38. R. Granek, M.E. Cates, *J. Chem. Phys.* **96**, 4758 (1992).